**4B.6**  EVOLUTION OF LOW-WAVENUMBER VORTICITY DURING RAPID INTENSIFICATION:
A DUAL-DOPPLER ANALYSIS

Matthew D. Eastin[*1], Paul D. Reasor[2], David S. Nolan[3], Frank D. Marks Jr.[4], John F. Gamache[4]

[1] Department of Math and Computer Science, Central College, Pella, Iowa
[2] Department of Meteorology, The Florida State University, Tallahassee, Florida
[3] Rosentiel School of Marine and Atmospheric Science, University of Miami, Miami, Florida
[4] NOAA/AOML Hurricane Research Division, Miami, Florida

## 1. INTRODUCTION

The azimuthal distribution of deep convection in a tropical cyclone inner core often consists of multiple transient convective cells superimposed upon a more slowly-evolving low-wavenumber (symmetric and asymmetric) structure. Numerous observations and numerical simulations suggest such distributions are intimately linked to the environmental vertical wind shear and internal dynamical processes (Reasor et al. 2000; Black et al. 2002; Corbosiero et al. 2006; Kossin and Schubert 2001; Braun 2002). Understanding the dynamics of the asymmetries is of fundamental importance due their influence not only on storm structure, but also storm motion (Nolan et al. 2000) and intensity (Moller and Montgomery 2000). The vertical shear will induce a wavenumber-one asymmetry with enhanced convergence and ascent downshear (Frank and Ritchie 1999, 2001). The higher-order asymmetries appear to be related to internal dynamics. In particular, intensifying tropical cyclones often exhibit an annular tower (or ring) of vertical vorticity with enhanced values in the eyewall and relatively depressed values in the eye and outside the eyewall (Kossin and Eastin 2001). Schubert et al. (1999) showed that such vorticity distributions are barotropically unstable whereby counterpropagating vortex Rossby waves (VRWs) could become phase-locked, grow in amplitude, and eventually break-down into coherent pools of vorticity, or "mesovortices". Depending on the initial structure of the vorticity ring, the mesovortices either merge and relax to a monopole, or remain distinct and form a quasi-steady rotating lattice (Kossin and Schubert 2001). In either case, the winds associated with the mesovortices exchanged considerable mass between the eye and eyewall. Eastin et al. (2005) recently presented observational evidence suggesting the mesovortices may help generate asymmetric buoyant convection via the transfer of high entropy air from the low-level eye into the relatively low-entropy eyewall, and thus contribute to storm evolution. Unfortunately, previous attempts to document the structure and evolution of these

*Corresponding Author Address:* Matthew D. Eastin, Department of Math and Computer Science, Central College, 812 University, Pella, IA 50219; email: eastinm@central.edu

Table 1: Dual-Doppler composite times for the 10 passes through Hurricane Guillermo on 02 August 1997 and the NOAA WP-3D aircraft (N42RF and N43RF) flight tracks across the inner core.

| Pass | Composite Time (UTC) | N42RF track (3.0 km) | N43RF track (5.8 km) |
|---|---|---|---|
| 1 | 1845-1905 | E to W | N to S |
| 2 | 1925-1944 | S to N | E to W |
| 3 | 1953-2010 | NW to SE | |
| 4 | 2033-2052 | NE to SW | |
| 5 | 2106-2129 | SE to NW | SW to NE |
| 6 | 2144-2159 | SW to ENE | NW to SE |
| 7 | 2215-2234 | NNE to SSW | |
| 8 | 2249-2307 | SE to NW | |
| 9 | 2324-2341 | SW to NE | SE to NW |
| 10 | 2354-2412 | NW to SE | SW to NE |
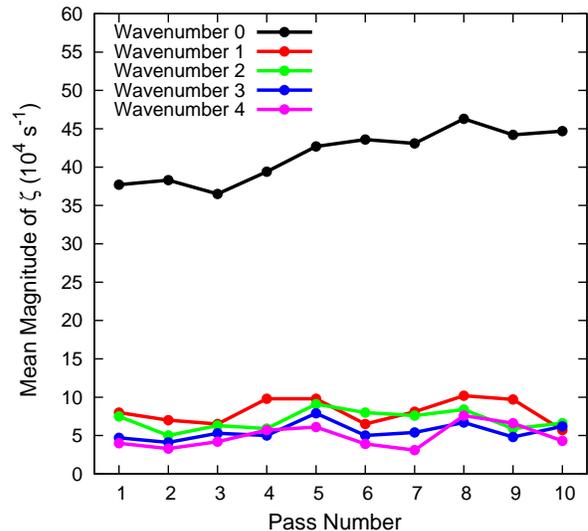


Figure 1: Azimuthal mean magnitude of the dual–Doppler-derived vertical vorticity averaged within the 10-25 km annulus between 1-3 km altitude of each composite wind field. Shown are the symmetric and azimuthal wavenumbers 1-4 contributions.

eye-eyewall mesovortices using Doppler radar were limited by insufficient data within the eye and large temporal gaps between composite wind fields. The objective of this study is to document the the three-dimensional structure and evolution of low-wavenumber vorticity in a *rapidly intensifying* tropical cyclone through the aid of a unique dual-Doppler dataset with considerably fewer limitations.

## 2.  DATA AND METHODS

Two NOAA WP-3D aircraft observed the inner core of Hurricane Guillermo between 1800 and 2400 UTC on 2 August 1997. During this period, the hurricane was moving westward over $> 29°C$ waters and intensifying at an average rate of 2.4 mb hr$^{-1}$ from an initial central pressure of 959 mb. Dual-Doppler velocity data was collected for ten passes through the inner core at 3.0 and 5.8 km altitude (Table 1). During dual-aircraft passes, the upper aircraft employed the fore-aft scanning technique (FAST) while the lower aircraft used a normal-plane scanning strategy. During single-aircraft passes the radar scanned in FAST mode. Unique three-dimensional wind fields were constructed for each

pass following Gamache (1998). The wind fields were decomposed into azimuthal mean and perturbation components following methods similar to Reasor et al. (2000). In contrast to previous Doppler radar studies of intense tropical cyclones, shallow convection and light precipitation within Guillermo's eye has permitted unprecedented wind field documentation throughout a large fraction of the low-level eye.

## 3.  RESULTS AND DISCUSSION

Figure 1 shows the azimuthal mean magnitudes of the symmetric and azimuthal wavenumbers 1-4 components of vorticity within the 10-25 km annulus between 1-3 km altitude for each pass, encompassing the mean eye-eyewall interface region inward of the radius of maximum wind (RMW). The symmetric component of vorticity dominated the region at all times and tended to increase with time. However, during two periods (Passes 2-3 and 6-7) the symmetric component decreased while higher wavenumber components increased in magnitude.

Figures 2 and 3 show the azimuthal mean (or symmetric) vorticity profiles at 3 km altitude for
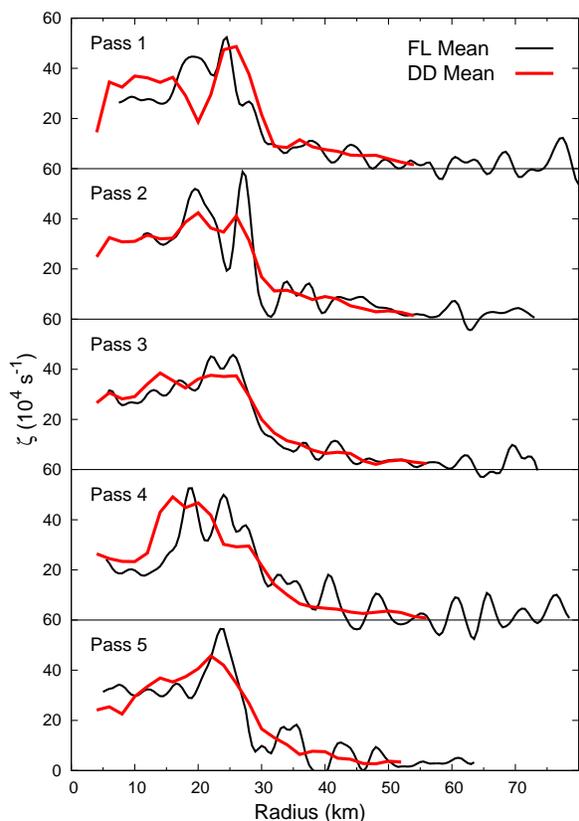


Figure 2: Azimuthal mean vorticity at 3 km altitude for Passes 1-5 computed from the flight-level data (black) and dual-Doppler composite winds (red).
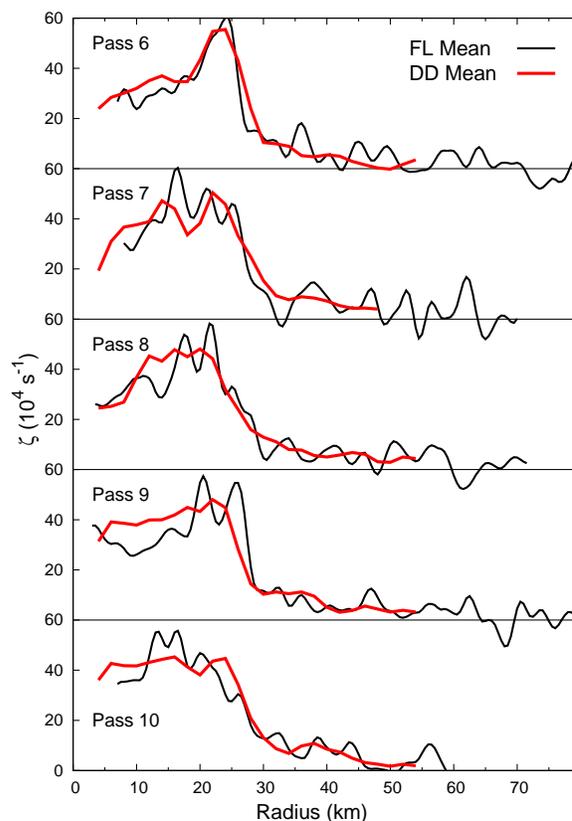


Figure 3: Azimuthal mean vorticity at 3 km altitude for Passes 6-10 computed from the flight-level data (black) and dual-Doppler composite winds (red).

each pass, computed from both the Doppler wind fields as well as flight-level data. Despite the resolution differences (0.5 and 2.0 km) and flight-level means comprised of only two radial legs, the respective profiles show good agreement at each time. Initially (Pass 1), the symmetric structure consisted of a ring with maximum values in the eyewall (at 25 km). During the next three passes, the eyewall maximum decreased while the vorticity along the eye-eyewall boundary (10-20 km) generally increased. A smaller increase was also apparent outside the initial maximum (near 30 km) by Pass 4. Such evolution is consistent with a breakdown of the vorticity ring into mesovortical structures as discussed above. During Passes 4 and 5 the mean eyewall vertical velocity significantly increased as a result of several deep convective bursts (not shown). Concurrently, a pronounced ring of enhanced symmetric vorticity re-emerged in the eyewall, reaching a maximum during Pass 6. Over the course of the the next four passes (7-10) the eyewall maximum decreased while vorticity inside the eye and just outside the eyewall increased. Again, such evolution is consistent with a vorticity ring breakdown into mesovortical structures. However, unlike the previous apparent breakdown, the profile relaxed to a monopole (Pass 10). Kossin and Eastin (2001) noted that such transitions frequently occurred after maximum intensity, marking the end of intensification, but they did not find *robust* evidence of episodic transitions during intensification. Clearly, the Guillermo profiles depict an evolving symmetric (and asymmetric) vorticity structure *during* rapid intensification.

Estimates of the environmental vertical wind shear vector computed as the difference in mean wind (within 50 km from the center) between the 8-10 km and 1-3 km altitude layers are shown in Fig. 4 for each pass. A persistent 6-7 m s$^{-1}$ north-northwesterly vertical shear was impinging on the

hurricane throughout the observation period. Such shear resulted from 3-4 m s$^{-1}$ southeasterly low-level flow and 4-5 m s$^{-1}$ northeasterly upper-level flow. Note the similarity between the mean dual-Doppler-derived vector and the estimated shear from the SHIPS predictor database (DeMaria and Kaplan 1999). During each pass, low-level convergence maxima were often located in the southern eyewall (downshear) with upward vertical velocity (and
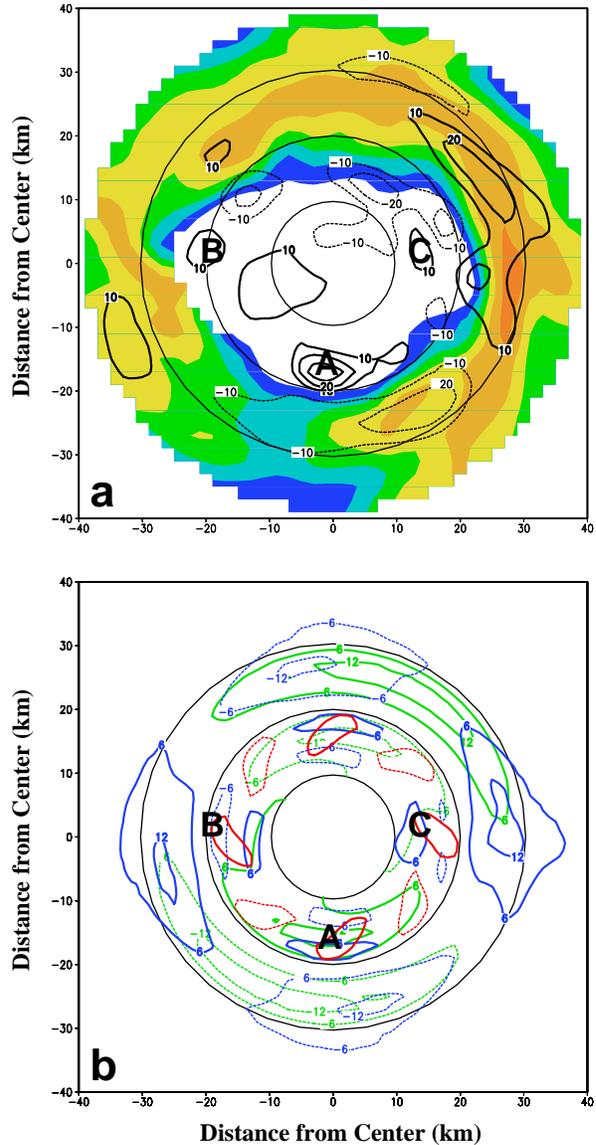
Figure 5: (a) Total perturbation vorticity (black) and (b) azimuthal wavenumber 1 (green), wavenumber 2 (blue), and wavenumber 4 (red) components of vorticity at 2 km altitude for Pass 2. The contour interval is 6 ×10-4 s-1 and negative values are depicted by dashed lines. Shaded contours show the 10, 15, 20, 25, 30, and 35 dBZ levels. The 10, 20, and 30 km range rings are also shown. Letters denote "mesovortices" discussed in the text.

Figure 4: Estimates of the environmental vertical wind shear vector computed from each Doppler wind field (black arrows) as the difference in mean wind (within 50 km from the center) between the 8-10 km and 1-3 km altitude layers (upper minus lower). Also shown is the mean shear vector of the 10 passes (green) and the 200-850 mb shear vector from the SHIPS predictor database (red).

radar reflectivity) maxima located in the southern and eastern eyewall (down and left of shear). This azimuthal structure is consistent with the aforementioned expected response of a vortex to northerly vertical shear.

The remaining discussion focuses on Passes 2, 3, and 4 during the first apparent vorticity ring breakdown. Figures 5-7 show the radar reflectivity, total perturbation vorticity, and the wavenumber 1, 2, and 4 components of vorticity at 2 km altitude for each of these passes. The eyewall reflectivity exhibited an elliptical shape with its major axis initially oriented west-east (Pass 2, Fig. 5a), then north-south (Pass 3, Fig. 6a), and finally west-east (Pass 4, Fig. 7a). Examination of reflectivity animations from the lower-fuselage radar suggests that the major axis rotated 90° cyclonically between each

composite's temporal midpoint. Superimposed on this elliptical structure were higher-wavenumber features, most notably a wavenumber-four structure evident along the eye-eyewall boundary (10 dBZ contour) during Pass 3. The total perturbation vorticity fields exhibit a structure rich with several coherent mesovortices. The majority are located 10-25 km from the circulation center with maximum vorticity values of 20-40 $\times 10^{-4}$ s$^{-1}$.

Two persistent, quasi-stationary, wavenumber-one vorticity maxima were observed during each pass (Figs. 5-7b). The outer (inner) maximum was located in the northeast eyewall (southwest eye) at 20-30 km (10-20 km) radius. While an erroneous wavenumber-one structure could arise from a center mislocation, both maxima were fairly robust during initial sensitivity tests.
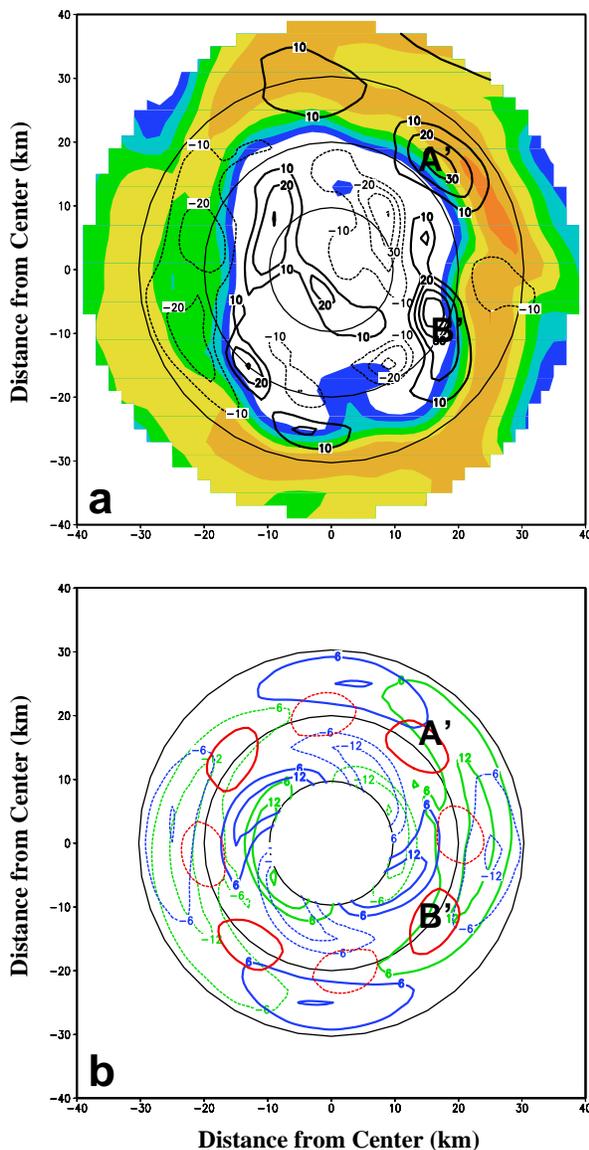


Figure 6: As in Fig. 5 except for Pass 3.
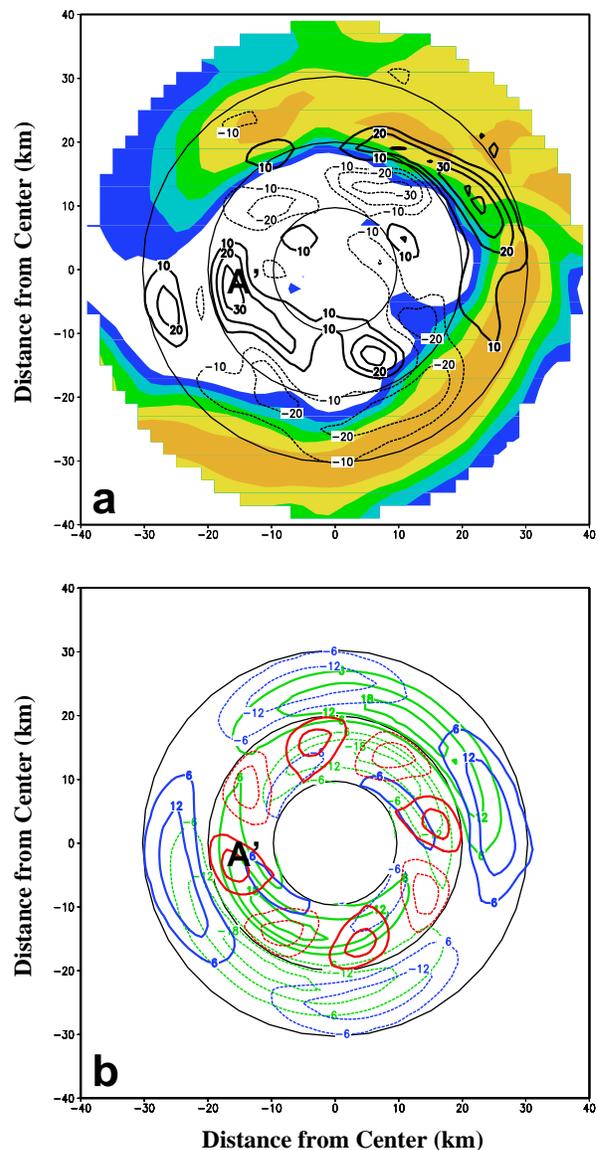


Figure 7: As in Fig. 5 except for Pass 4.

The dominant wavenumber-two vorticity structure was located in the eyewall at 20-30 km radius. Maximum vorticity values were approximately 10-15 $\times 10^{-4}$ s$^{-1}$ and increased with time. The positive asymmetries were initially oriented west-east (Pass 2), then north-south (Pass 3), and finally west-east (Pass 4) in manner consistent with the major axis of the elliptical reflectivity structure. Such evolution may be indicative of a propagating wavenumber-two VRW. According to linear theory, the phase speed of a wavenumber-two vortex-Rossby edge wave is one half the maximum tangential wind. During this time period the Vmax and RMW at 3 km altitude were 48 m s$^{-1}$ and 28 km, respectively. The circulation period for a wavenumber-two edge wave would then be 122 min. With a temporal resolution of ~30 min between composite midpoints, the observed 90° cyclonic rotation is consistent. Similar results have been found by Kuo et al. (1999), Reasor et al. (2000), and Corbosiero et al. (2006).

The wavenumber-three vorticity component (not shown) was relatively weak and inconsistent during Passes 2-4. However, more persistent structures were evident at later time periods.

A prominent wavenumber-four vorticity structure was observed along the eye-eyewall boundary at ~20 km radius. Maximum vorticity values were approximately 8-14 $\times 10^{-4}$ s$^{-1}$ and increased with time. A close comparison of the total perturbation and wavenumber-four fields reveals that several coherent mesovortices (both positive and negative) are collocated with wavenumber-four anomalies of similar sign. Three such examples during Pass 2 (Fig. 5) are marked with the letters A, B, and C. In relation to the reflectivity structure, the orientation of the positive anomalies was roughly 10-20° cyclonically downwind of each outward protrusion of low ($< 10$ dBZ) reflectivities. This relationship was most apparent during Pass 3 (Fig. 6) and is consistent with the expectations of differential hydrometeor advection associated with the mesovortical flow. Furthermore, radar animations show these protrusions rotating cyclonically "through" the elliptical structure. Using linear wave theory as a guide, a wavenumber-four vortex Rossby wave should rotate at ~75% of the local tangential wind, or ~50% faster than a wavenumber-two wave.

Are these mesovortices wavenumber-four VRWs? At the time of Pass 2 (Fig. 5), mesovortex A was located 18 km due south of center with a local tangential wind of ~35 m s$^{-1}$. In the ~30 min between the composite midpoints of Passes 2 and 3, linear theory predicts a wavenumber-four VRW would rotate ~150° cyclonically around the vortex to the northeast. The mesovortex observed 24 km northeast of center (labeled A' in Fig. 6) and nearly collocated with a positive wavenumber-four vorticity maximum is consistent with such motion. Following the same procedure for this mesovortex, linear theory predicts a wavenumber-four VRW would be located ~20 km west of center by the fourth pass. Again, the mesovortex observed 18 km west of center

(labeled A' in Fig. 7) and collocated with a positive wavenumber-four vorticity maximum is consistent. Furthermore, note that the mesovortex located ~20 km west-northwest of center during Pass 2 (labeled B in Fig. 5) and the mesovortex located ~18 km southwest of center during Pass 3 (labeled B' in Fig. 6) is also consistent with the expected behavior of a wavenumber-four VRW.

Our preliminary results indicate that the low-wavenumber vorticity structure of a rapidly intensifying tropical cyclone can be quite dynamic. In particular, two episodes of vorticity ring breakdown (into mesovortices) appear to have occurred during rapid intensification, and the associated evolution of higher-wavenumber mesovortices appears consistent with the expectations of vortex-Rossby waves. Ongoing work involves a complete documentation of the structure and evolution of the mesovortices associated with both episodes, as well as vorticity structures at upper levels. Future work will also attempt to reconcile the observed convective structure within the context of the evolving low-wavenumber vorticity features as they interact with the quasi-stationary vertical shear forcing.

## REFERENCES

Black, M. L., J. F. Gamache, F. D. Marks, Jr., C. E. Samsury, and H. E. Willoughby, 2002: Eastern Pacific Hurricanes Jimena of 1991 and Olivia of 1994: The effect of vertical shear on structure and intensity. *Mon. Wea. Rev.*, **130**, 2291-2312.

Braun, S. A., 2002: A cloud-resolving simulation of Hurricane Bob (1991): Storm structure and eyewall buoyancy. *Mon. Wea. Rev.*, **130**, 1573-1592.

Corbosiero, K. L., J. Molinari, A. R. Aiyyer, and M. L. Black, 2006: The structure and evolution of Hurricane Elena (1995). Part II: Convective asymmetries and evidence for vortex-Rossy waves. Submitted to *Mon. Wea. Rev.*.

DeMaria, M., and J. Kaplan, 1999: An updated statistical hurricane intensity prediction scheme (SHIPS) for the Atlantic and eastern North Pacific basin. *Wea. Forecasting*, **14**, 326-337.

Eastin, M. D., W. M. Gray, and P. G. Black, 2005: Buoyancy of convective vertical motions in the inner core of intense hurricanes. Part II: Case Studies. *Mon. Wea. Rev.*, **133**, 209-227.

Frank, W. M., and E. A. Ritchie, 1999: Effects of environmental flow upon tropical cyclone structure. *Mon. Wea. Rev.*, **127**, 2044-2061.

Frank, W. M., and E. A. Ritchie, 2001: Effects of vertical wind shear on the intensity and structure of numerically simulated hurricanes. *Mon. Wea. Rev.*, **129**, 2249-2269.

Gamache, J. F., 1998: Evaluation of a fully three-dimensional variational Doppler analysis tech-

nique. Preprints, *28th Conf. on Radar Meteorology*, Austin, TX, Amer. Meteor. Soc., 422-423.

Kossin, J. P., and M. D. Eastin, 2001: Two distinct regimes in the kinematic and thermodynamic structure of the hurricane eye and eyewall. *J. Atmos. Sci.*, **58**, 1079-1090.

Kossin, J. P., and W. H. Schubert, 2001: Mesovortices, polygonal flow patterns, and rapid pressure falls in hurricane-like vortices. *J. Atmos. Sci.*, **58**, 2196-2209.

Kuo, H.-C., R. T. Williams, and J.-H. Chen, 1999: A possible mechanism for the eye rotation of Typhoon Herb. *J. Atmos. Sci.*, **56**, 1659-1673.

Moller, J. D., and M. T. Montgomery, 2000: Tropical cyclone evolution via potential vorticity anomalies in a three-dimensional balance model. *J. Atmos. Sci.*, **57**, 3366-3387.

Nolan, D. S., M. T. Montgomery, and L. D. Grasso, 2001: The wavenumber-one instability and trochoidal motion of hurricane-like vortices. *J. Atmos. Sci.*, **58**, 3243-3270.

Reasor, P. D., M. T. Montgomery, F. D. Marks Jr., and J. F. Gamache, 2000: Low-wavenumber structure and evolution of the hurricane inner core observed by airborne dual-Doppler radar. *Mon. Wea. Rev.*, **128**, 1653-1680.